Applied Catalysis B: Environmental 239 (2018) 309–316

Contents lists available at ScienceDirect

Applied Catalysis B: Environmental

journal homepage: www.elsevier.com/locate/apcatb

Scalable fabrication of $Zn_xCd_{1-x}S$ double-shell hollow nanospheres for highly efficient hydrogen production

Chenyang Zhang[a], Huanhuan Liu[b], Wanni Wang[a], Haisheng Qian[a,c,*], Sheng Cheng[d], Yang Wang[d], Zhengbao Zha[a], Yijun Zhong[b,e], Yong Hu[b,e,**]

[a] School of Biological and Medical Engineering, School of Food Science and Engineering, Hefei University of Technology, Hefei, 230009, PR China
[b] Key Laboratory of the Ministry of Education for Advanced Catalysis Materials, Department of Chemistry, Zhejiang Normal University, Jinhua 321004, PR China
[c] Biomedical and Environmental Interdisciplinary Research Centre, Hefei, 230010, PR China
[d] Instrumental Analysis Center, Hefei University of Technology, Hefei 230009, PR China
[e] Hangzhou Institute of Advanced Studies, Zhejiang Normal University, Hangzhou 311231, PR China

ARTICLE INFO

Keywords:
$Zn_xCd_{1-x}S$ double-shell hollow nanospheres
Growth mechanism
Sacrificial template method
Hydrogen production

ABSTRACT

Hollow nanostructures are of great scientific and technological importance for extensive applications in photocatalysis, drug delivery, wastewater treatment, etc. In this study, we have developed a facile hydrothermal method for the large scale fabrication of alloyed $Zn_xCd_{1-x}S$ double-shell (DS-$Zn_xCd_{1-x}S$) hollow nanospheres using hierarchically porous ZnS nanospheres as sacrificial templates and the reagent $Cd(Ac)_2$ as a Cd source. The growth mechanism of double-shell hollow nanospheres has been studied and illustrated by investigating the morphological evolution of the inter-mediated products. Moreover, the chemical composition and void space between the double-shells of the as-obtained alloyed $Zn_xCd_{1-x}S$ hollow nanospheres can be regulated by adding a certain amount of $Cd(Ac)_2$. The optical properties and band structures have been investigated using UV–vis diffuse reflectance spectroscopy (DRS), Mott-Schottky analysis and valence-band (VB) X-ray photoelectron spectroscopy, respectively. When evaluated for their photocatalytic properties, the as-prepared alloyed $Zn_{0.46}Cd_{0.54}S$ double-shell (DS-$Zn_{0.46}Cd_{0.54}S$) hollow nanospheres exhibit excellent hydrogen production, and a H_2 evolution speed of up to 4.11 mol h^{-1} g^{-1} is reached under irradiation of visible light ($\lambda > 420$ nm).

1. Introduction

Hollow nanostructures have attracted extensive attention due to their great structural advantages, such as low density, high specific surface area and high loading capacity [1–7], which have led to promising potential applications in drug delivery [8–11], catalysis [12–18], energy storage and conversion [19–24], and so on. Thus, considerable efforts have been made to design and construct various hollow nanostructures by means of different synthetic strategies, for instance, chemical vapor deposition [25,26], layer-by-layer coating technique [27–33], the template-engaged replacement reaction [34–36], and surfactant micellar templating [37–42]. In general, templating has been recognized as one of the most important techniques for fabricating hollow nanostructures after removing the templates via reaction or etching techniques, which involves using hard, soft or self-sacrificial templates. Lou and co-workers developed a sequential ion-change strategy to prepare onion-like $NiCo_2S_4$ with unique hollow structured shells using a precursor of onion-like metal oxide particles, which exhibit superior electrochemical performance for hybrid supercapacitors with outstanding cycle life and enhanced energy/power densities due to their unique shell architecture and robust matrix [43]. Recently, Lou et al. fabricated multi-shelled various alloy oxide hollow spheres through a penetration-solidification-annealing method, including $CoMn_2O_4$, $Co_{1.5}Mn_{1.5}O_4$, $MnCo_2O_4$, $ZnMn_2O_4$, $ZnCo_2O_4$, and $NiCo_2O_4$ [44]. Wang et al. developed a sequential templating approach to fabricate metal ferrite (MFe_2O_4, M = Zn, Co, Ni, Cd) [45], ZnO [46], TiO_2 [47], Co_3O_4 [48], α-Fe_2O_3 [49], MnO_x [50], SnO_2 [51], V_2O_5 [52], and $(Co_{2/3}Mn_{1/3})(Co_{5/6}Mn_{1/6})_2O_4$ [53] multi-shelled hollow nanospheres utilizing carbonaceous microspheres as sacrificial templates.

Transition metal sulfides have received significant attention as

* Corresponding author at: School of Biological and Medical Engineering, School of Food Science and Engineering, Hefei University of Technology, Hefei, 230009, PR China.
** Corresponding author at: Key Laboratory of the Ministry of Education for Advanced Catalysis Materials, Department of Chemistry, Zhejiang Normal University, Jinhua 321004, PR China.
E-mail addresses: shqian@hfut.edu.cn (H. Qian), yonghu@zjnu.edu.cn (Y. Hu).

https://doi.org/10.1016/j.apcatb.2018.08.027
Received 2 May 2018; Received in revised form 15 July 2018; Accepted 13 August 2018
Available online 14 August 2018

promising electrode materials with high-performance for energy storage devices. Meanwhile, binary alloy sulfides possess higher capacity, chemical stability and higher electrochemical activity than single metal sulfides [54–56]. More recently, Lou et al. demonstrated a moderate anion exchange method to fabricate ternary ball-in-ball-like hollow nanostructures of $NiCo_2S_4$ for enhanced electrochemical pseudocapacitive properties [57]. Despite the many efforts concentrated on synthesizing highly complex binary alloy sulfides, developing a facile process to synthesize hollow binary alloy sulfides with high quality on the large scale is still a challenging task.

Herein, we demonstrate a simple synthetic strategy for the large-scale fabrication of alloyed double-shell (DS-$Zn_xCd_{1-x}S$) hollow nanospheres via a sacrificial template route and hierarchically porous ZnS nanospheres used as hard templates. In the proposed process, a layer of CdS promptly formed at the surface of hierarchically porous ZnS nanospheres, whereas small nanoparticles of ZnS disassemble from the hierarchically porous ZnS nanospheres and dissolved gradually. The pre-synthesized CdS layer will convert to $Zn_xCd_{1-x}S$ via a solution-crystallization process, resulting in the formation of double-shell hollow nanostructures of $Zn_xCd_{1-x}S$, and the proposed synthetic strategy is illustrated in Scheme 1. Furthermore, the synthetic mechanism of the DS-$Zn_xCd_{1-x}S$ hollow nanospheres has been extensively studied. Benefiting from the extraordinary structural features, the as-obtained alloyed DS-$Zn_{0.46}Cd_{0.54}S$ hollow nanospheres exhibit excellent hydrogen production under visible-light illumination ($\lambda > 420$ nm).

2. Materials and methods

All chemicals were of analytical grade and used without further purification

2.1. Scalable synthesis of AA-$[Zn(OH)_4]^{2-}$ complex nanospheres

In a typical synthesis route, 7.2 mmol of CTAB and 0.72 mmol of AA were added into a 250 ml round-bottom flask and dissolved using 150 ml deionized water. Subsequently, 2.7 mmol of $Zn(NO_3)_2{\cdot}6H_2O$ and 2.7 mmol of HMTA were introduced into the solution with vigorously stirred for 30 min before being heated and maintained at 85 °C for 10 h. The resulting milky white suspension was washed three times with deionized water and absolute ethanol, and then dried at 50 °C for 24 h. Finally, the AA-$[Zn(OH)_4]^{2-}$ complex was obtained.

2.2. Scalable fabrication of hierarchically porous ZnS complex

Briefly, hydrogen sulfide gas was produced from dilute H_2SO_4 and excess $Na_2S{\cdot}9H_2O$ using a simple experimental installation, which was introduced into a vacuum bottle containing the as-obtained AA-$[Zn(OH)_4]^{2-}$ powder complex. The vacuum bottle was heated to 60 °C and maintained for 4 h. Then, the sample was washed several times with deionized water and absolute ethanol and dried at 60 °C.

2.3. Preparation of $Zn_xCd_{1-x}S$ double-shell hollow nanospheres

Typically, to synthesize $Zn_{0.46}Cd_{0.54}S$ double-shell hollow nanospheres, 0.24 g of as-obtained hierarchically porous ZnS and 4.86 mmol of cadmium acetate were loaded in a 250 ml beaker containing 60 ml of distilled water and stirred for 20 min to form a milky solution. Then, 40.5 mmol of a thiourea aqueous solution was dropped into the above mixture. After stirring for 10 min, the mixture was put into a 100 ml Teflon-lined stainless-steel autoclave, sealed and maintained at 140 °C for 4 h. Subsequently, cooling down to room temperature naturally, and the final product was collected by centrifugation and washed with distilled water and absolute ethanol several times. Analogously, the as-prepared $Zn_xCd_{1-x}S$ (x = 1.0, 0.59 and 0.32) products have been synthesized from different amounts of cadmium acetate while the other conditions were kept constant. Atomic absorption spectroscopy (AAS) has been used to decide the accurate mole ratio of Zn/Cd.

2.4. Characterizations

Morphology of these products was investigated using field-emission scanning electron microscopy (FESEM) and transmission electron microscopy (TEM), respectively. The field-emission scanning electron microscopy (FESEM) images were recorded on a SU8020 (Hitachi, Japan); transmission electron microscopy (TEM) and high-resolution transmission electron microscopy (HRTEM) images were obtained using a JEM-2100 F (JEOL, Japan). Powder X-ray diffraction (XRD) patterns were determined by using an X'Pert PRO MPD X-ray diffractometer (PANalytical B.V., Holland) equipped with graphite monochromated Cu Kα radiation. X-ray photoelectron spectra (XPS) were performed on an ESCALAB250Xi X-ray photoelectron spectrometer (Thermo Scientific, American). UV–vis absorption spectra were recorded by using a Hitachi U-5100 spectrophotometer (Hitachi High-Technology Corporation). Fluorescent spectra were studied with a fluorescence spectrometer (Edinburgh FLS980, UK). The UV–vis diffuse reflectance spectra (UV–vis DRS) of the as-obtained solid samples were taken using a CARY 5000 (Agilent Technology Corporation). Fourier transform infrared (FTIR) spectra of the as-prepared samples were collected by a Nicolet 67 (Thermo Nicolet, American). The mole ratio of Zn/Cd was measured by using AA800 atomic absorption spectrometer (AAS, Perkin Eimei, American). The nitrogen sorption isotherm was conducted by using an automatic volumetric adsorption apparatus (Micromeritics ASAP 2020).

3. Results and discussion

First, AA-$[Zn(OH)_4]^{2-}$ complex nanospheres were prepared from $Zn(NO_3)_2{\cdot}6H_2O$, l-ascorbic acid (AA), Cetyltrimethylammonium bromide (CTAB) and hexamethylenetetramine (HMTA) at 85 °C on a large scale and converted to ZnS via gas sulfidation. Fig. 1a, b reveals TEM images of the as-obtained AA-$[Zn(OH)_4]^{2-}$ complex, indicating that the product completely consisted of monodisperse nanospheres approximately 230 nm in diameter, which could be further verified by the FE-SEM image displayed in Fig. S1. From Fig. 1c, the XRD pattern of the as-prepared AA-$[Zn(OH)_4]^{2-}$ complex demonstrates that the AA-$[Zn(OH)_4]^{2-}$ precursor is amorphous. Fig. 1d displays TEM image of the product after sulfidation of the AA-$[Zn(OH)_4]^{2-}$ complex product. In addition, the as-prepared ZnS composite nanospheres were comprised of small nanoparticles several nanometres in size and with a porous structure, which is derived from the aggregation and hydroxyl elimination of the AA-$[Zn(OH)_4]^{2-}$ complex during the sulfidation process (Fig. 1e). The ZnS nanoparticles possess an average diameter of 5.8 nm,

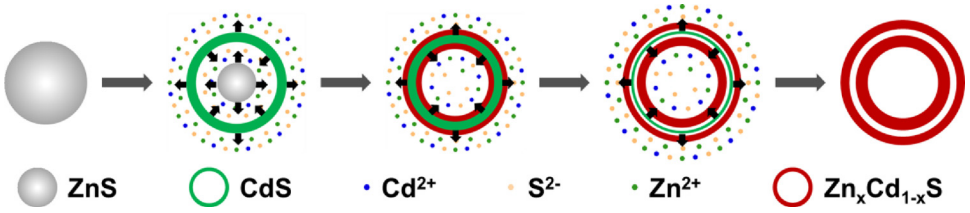

Scheme 1. Schematic illustration of the synthetic strategy of the $Zn_xCd_{1-x}S$ double-shell hollow nanospheres.

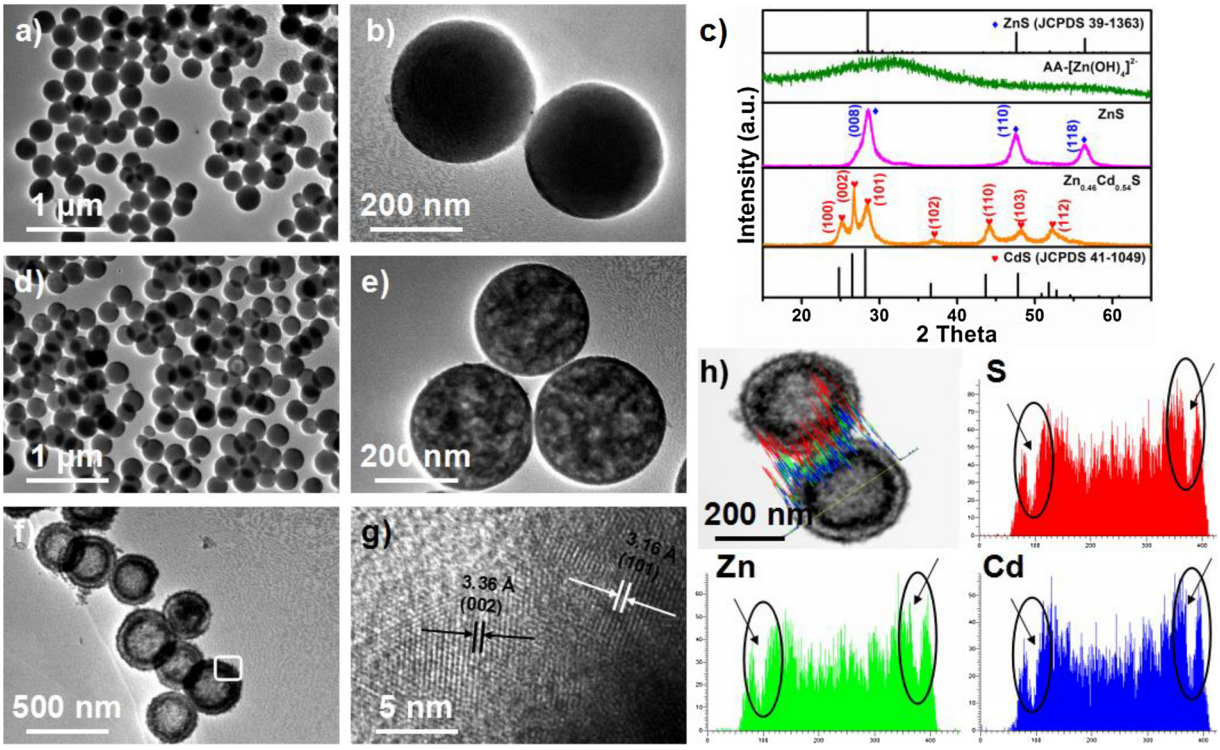

Fig. 1. (a, b) TEM images of AA-$[Zn(OH)_4]^{2-}$ composite nanospheres; (c) XRD patterns of the as-obtained products; (d, e) TEM images of ZnS composite nanospheres; (f, g) TEM and HRTEM images of DS-$Zn_{0.46}Cd_{0.54}S$ hollow nanospheres; (h) the STEM image of DS-$Zn_{0.46}Cd_{0.54}S$ hollow nanospheres and EDS line scan for the elemental distribution.

which is estimated from XRD data (Fig. 1c) according to the Scherrer equation ($Rm = k\lambda/\beta_{1/2}\cos\theta$), which agrees well with the morphological analysis. As shown in Fig. S2, Brunauer-Emmett-Teller (BET) surface area analysis indicates that the ZnS composite nanospheres have a specific surface area of 60.32 $m^2 g^{-1}$, implying ZnS nanospheres with hierarchically porous structures, which can be further verified by thermal gravimetric analysis (TGA) due to the removal of some organics after sulfidation of the AA-$[Zn(OH)_4]^{2-}$ complex product (Fig. S3) [58]. Fig. 1f shows the TEM image of the as-prepared final sample obtained from 0.24 g of as-obtained hierarchically porous ZnS nanospheres, 4.86 mmol of cadmium acetate and 40.5 mmol of thiourea at 140 °C for 4 h, which is composed of double-shell hollow nanospheres with a total diameter of 360 nm and a shell thickness of several nanometres; the distance between the double-shells is approximately 32 nm, as observed from the TEM image. From the high-resolution TEM image of the selected outer shell section, as shown in Fig. 1g, the lattice fringes of 3.36 and 3.16 Å can be easily indexed to the (002) and (110) crystal planes of hexagonal $Zn_xCd_{1-x}S$. Moreover, the lattice fringes are slightly smaller than the interplanar distance of pure CdS, demonstrating the formation of alloyed $Zn_xCd_{1-x}S$ nanostructures. The XRD pattern for the final sample also confirmed the formation of hexagonal alloyed $Zn_xCd_{1-x}S$ (Fig. 1c). The energy dispersive spectroscopy (EDS) line scan for the elemental distribution is shown in Fig. 1h, indicating that the hollow nanospheres have a double-shell structure. Fig. S4 shows scanning transmission electron microscopy (STEM)-EDS analysis of the as-prepared sample, which illustrates that the elements of Zn, S and Cd ingredient homogeneously distribute, implying the formation of alloyed DS-$Zn_{0.46}Cd_{0.54}S$ hollow nanospheres. XPS of the as-prepared DS-$Zn_{0.46}Cd_{0.54}S$ hollow nanospheres verifies the elements in the final samples, including Zn, Cd, S and their chemical states (Fig. S5). The accurate chemical composition was investigated using AAS, and the alloyed double-shell hollow nanosphere has a Zn/Cd mole ratio of 0.46/0.54. Hence, based on the above analysis of the morphology, phase and chemical composition, DS-$Zn_{0.46}Cd_{0.54}S$ hollow nanospheres have been synthesized using the present synthetic strategy.

The morphological evolution of the as-prepared DS-$Zn_{0.46}Cd_{0.54}S$ hollow nanospheres in the preliminary stages was used to confirm the proposed synthetic mechanism for the formation of double-shell hollow nanospheres, as revealed by these TEM images shown in Fig. 2a–c. Fig. 2a shows the TEM image of the sample obtained at 140 °C for 0.5 h in which hollow nanospheres with similar size have been clearly observed. In fact, many small nanoparticles several nanometres in size have been observed to exist in the inner hollow nanospheres. As demonstrated in Fig. S6, the STEM image and the elemental mapping images show that the shell is comprised of Zn, S and Cd elements. All these demonstrated that a thin layer of $Zn_xCd_{1-x}S$ was coated on the surface of the ZnS nanospheres at the earlier stage to form a tight hollow nanostructure. As a result, the dissolution and crystallization of ZnS nanoparticles made Zn^{2+} incorporate into the lattice of CdS to form $Zn_xCd_{1-x}S$ alloyed shell and alloyed $Zn_xCd_{1-x}S$ nanoparticles. The hierarchically porous ZnS nanospheres were comprised of many small nanoparticles several nanometres in size, which was stabilized by l-ascorbic acid molecules (AA), as displayed by the FTIR spectra (Fig. S7). The ZnS nanospheres should be disassembled into small nanoparticles (Fig. S8) under hydrothermal conditions owing to the dissolution and crystallization of ZnS nanoparticles, which promptly undergo coating with a lamina of CdS or $Zn_xCd_{1-x}S$ on the surface, and the ZnS porous nanospheres promptly disintegrated in the earlier stage. With a prolonged reaction time, the small nanoparticles of $Zn_xCd_{1-x}S$ or ZnS would gradually dissolve and crystallize on the inner or outer surface of a preformed thin layer of CdS or $Zn_xCd_{1-x}S$. Meanwhile, the inner CdS or $Zn_xCd_{1-x}S$ shell would dissolve and recrystallize by means of a diffusion mass transfer process to gradually form void interspace, resulting in the formation of double-shell hollow nanospheres (Fig. 2c). The XRD patterns of the intermediated products are revealed in Fig. 2d, in which all the diffraction peaks can be readily indexed to hexagonal $Zn_xCd_{1-x}S$, implying that ZnS porous nanospheres promptly converted to the $Zn_xCd_{1-x}S$ composition by reacting with Cd^{2+} and thiourea. Three

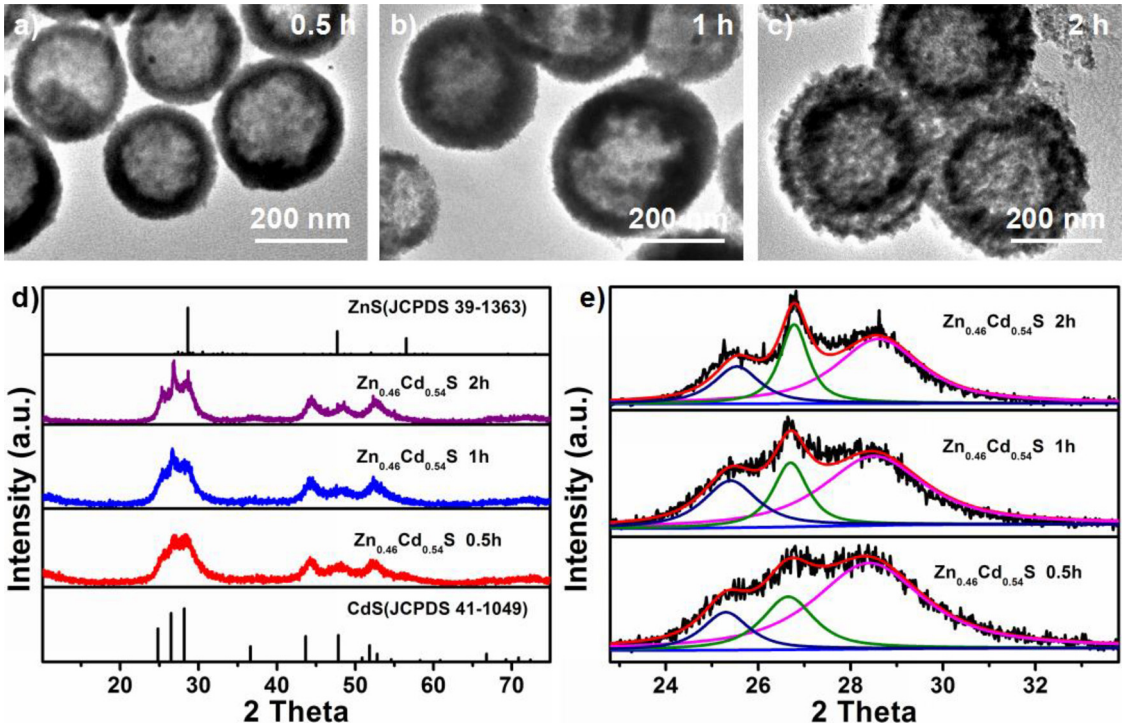

Fig. 2. (a–c) TEM images of the samples collected in the early stages of formation of DS-$Zn_{0.46}Cd_{0.54}S$ hollow nanospheres; (d, e) XRD patterns of the as-obtained products.

peaks located at 27° for hexagonal alloyed $Zn_xCd_{1-x}S$ can be analysed using a Gaussian curve, and the diffraction angles shifted slightly to higher values, demonstrating Zn ions doped the CdS lattice to form a stable $Zn_xCd_{1-x}S$ alloy (Fig. 2e) [59]. The chemical composition of the intermediated product was studied using XPS and AAS, respectively. The chemical composition of the intermediated product, shown in Table S1 and Table S2, demonstrates that the formed mechanism of DS-$Zn_{0.46}Cd_{0.54}S$ hollow nanospheres can be illustrated by the proposed strategy shown in Scheme 1.

In this case, the chemical composition can be modulated by controlling the concentration of $Cd(Ac)_2$. Fig. 3a–c shows the TEM images of the as-synthesized double-shell hollow spheres obtained from different amounts of $Cd(Ac)_2$ and other reaction factors were kept the same. The precise Zn/Cd mole ratios were determined as 0.59/0.41 (Fig. 3a) and 0.32/0.68 (Fig. 3c) by AAS when the quantity of $Cd(Ac)_2$ was adjusted to 2.43 mmol and 6.48 mmol, respectively. As shown in Fig. 3d, the distance between the double-shells varied and is dependent on the shell thickness of the CdS or $Zn_xCd_{1-x}S$ formed in the early stage. According to the formation mechanism of the double-shell hollow nanospheres, the amount of $Cd(Ac)_2$ acts a crucial role in forming the double-shell hollow nanospheres, which determine the reaction and formation speed or thickness of CdS or $Zn_xCd_{1-x}S$ layer at the early stage. When the quantity of $Cd(Ac)_2$ was decreased to 1.62 mmol and other reaction conditions were held constant, no double-shell hollow nanospheres were obtained, and only hollow nanospheres and some nanoparticles were clearly observed (Fig. S9a), which can be ascribed to the slow formation speed of the CdS or $Zn_xCd_{1-x}S$ thin layer. If the concentrations of $Cd(Ac)_2$ and thiourea were increased greatly, CdS nanoparticles not a CdS layer formed at the surface of the ZnS nanospheres. As shown in Fig. S9b, there are many small nanoparticles with an approximately average size of 20 nm obtained when the quantity of $Cd(Ac)_2$ and thiourea was simultaneously increased to 6.48 mmol and 60.8 mmol while other conditions were kept constant. Meanwhile, ethylene glycol was chosen as a system for the solvothermal reaction, and the amount of thiourea was reduced to 16.2 mmol to retard the reaction speed while other factors were kept constant, resulting in the successful synthesis of uniform high quality single-shell $Zn_{0.43}Cd_{0.57}S$ (SS-$Zn_{0.43}Cd_{0.57}S$) hollow nanospheres approximately 290 nm in diameter and 35 nm in shell thickness (Fig. S10a). As shown in Fig. S10b-e, the three elements of S, Zn, and Cd are identified in all the hollow nanospheres, indicating that all three elements are homogeneously distributed throughout the as-obtained SS-$Zn_{0.43}Cd_{0.57}S$ hollow nanospheres. The nanostructure of the as-prepared SS-$Zn_{0.43}Cd_{0.57}S$ hollow nanospheres was further confirmed by XRD. As revealed in Fig. S10f, the pattern of the sample also confirmed the formation of hexagonal alloyed SS-$Zn_{0.43}Cd_{0.57}S$ hollow nanospheres. To determine the microstructure of the DS-$Zn_{0.46}Cd_{0.54}S$ and SS-$Zn_{0.43}Cd_{0.57}S$ hollow nanospheres, BET measurements have been conducted (Fig. S11). The specific surface area of the DS-$Zn_{0.46}Cd_{0.54}S$ with 36.99 $m^2 g^{-1}$ is similar with that of SS-$Zn_{0.43}Cd_{0.57}S$ (36.57 $m^2 g^{-1}$), indicating DS-$Zn_{0.46}Cd_{0.54}S$ and SS-$Zn_{0.43}Cd_{0.57}S$ with similar nanostructures comprised of small nanoparticles which will provide reaction sites for the photocatalysis [60,61].

The optical physical properties of the as-synthesized $Zn_xCd_{1-x}S$ hollow nanospheres were evaluated using UV–vis absorbance spectra. Fig. S12 shows that the wide UV–vis absorption peaks of the as-obtained $Zn_xCd_{1-x}S$ hollow nanospheres were located at 373, 382, 394 and 442 nm, which can be assigned to the alloyed $Zn_xCd_{1-x}S$ nanostructures with different Zn/Cd ratios compared to those in the UV–vis absorption spectra of single ZnS and CdS [62–64]. The UV–vis DRS of the as-obtained double-shell hollow nanospheres are displayed in Fig. 4a, which agree well with the UV–vis absorption spectra. In addition, DS-$Zn_xCd_{1-x}S$ hollow nanospheres possessed a stronger light absorbance within the range of 550–800 nm than SS-$Zn_{0.43}Cd_{0.57}S$ hollow nanospheres due to the increase in the shell layer number, which could efficiently heighten the visible light harvesting capacity [65,66]. The band-gap energy of the as-obtained $Zn_xCd_{1-x}S$ hollow nanospheres at 300 K has been estimated from the Kubelka-Munk function $[F(R)h\nu]^2$ versus the photon energy ($h\nu$) [67]. As shown in Fig. 4b, the evaluated band-gap energy of the as-synthesized $Zn_xCd_{1-x}S$ (x = 0.59, 0.46, 0.43, 0.32) hollow nanospheres are 2.47, 2.39, 2.40, and 2.26 eV, respectively.

To better figure out band structures of the as-prepared products,

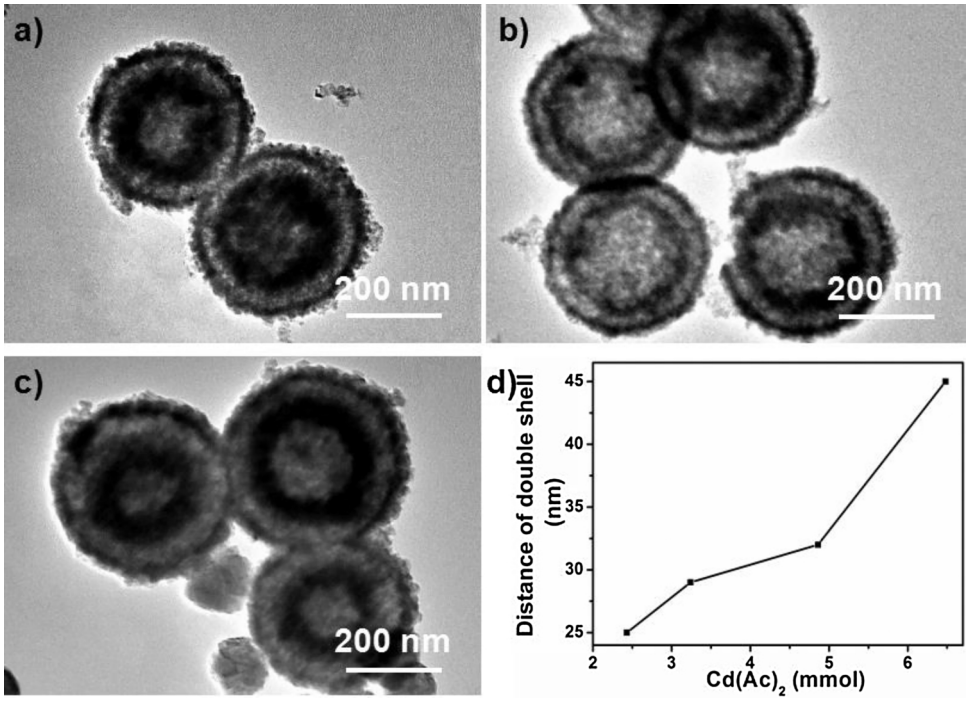

Fig. 3. (a–c) TEM images of as-prepared $Zn_xCd_{1-x}S$ hollow nanospheres with different chemical composition obtained using different amounts of $Cd(Ac)_2$: (a) 2.43 mmol; (b) 3.24 mmol; and (c) 6.48 mmol; (d) The dependence curve of the distance between of the two shells versus amount of $Cd(Ac)_2$.

Mott-Schottky measurement was further performed [68,69]. From the Mott-Schottky plots (Fig. S13), the conduction band (CB) of all the samples became more negative with the increase in the amount of Cd^{2+} ions. A more negative CB has a stronger reducing capacity, which contributes to an improved ability towards photocatalytic water reduction. From the results of the Mott-Schottky and UV–vis DRS, the CB and valence band (VB) energy levels for $Zn_xCd_{1-x}S$ hollow nanosphere photocatalysts are further illustrated in Fig. S14.

The photocatalytic performance of all the samples was illustrated by the hydrogen evolution reaction with co-catalysts Pt under visible-light irradiation ($\lambda > 420$ nm). As shown in Fig. 5a, different samples were used as photocatalysts to produce H_2. Obviously, the photocatalytic activity is in the order of SS-$Zn_{0.43}Cd_{0.57}S$ < DS-$Zn_{0.59}Cd_{0.41}S$ < DS-$Zn_{0.32}Cd_{0.68}S$ < DS-$Zn_{0.46}Cd_{0.54}S$. The H_2 evolution rate of DS-$Zn_{0.46}Cd_{0.54}S$ is 4.11 mol h^{-1} g^{-1}, which is nearly 2.22, 1.71, and 3.07 times higher than that of the DS-$Zn_{0.59}Cd_{0.41}S$ (1.85 mol h^{-1} g^{-1}), DS-$Zn_{0.32}Cd_{0.68}S$ (2.40 mol h^{-1} g^{-1}) and SS-$Zn_{0.43}Cd_{0.57}S$ (1.34 mol h^{-1} g^{-1}), respectively (Fig. 5b). Additionally, DS-$Zn_{0.46}Cd_{0.54}S$ hollow nanospheres could maintain their inherent photocatalytic activity without evident inactivation during three cycles (Fig. 5c), displaying excellent stability and reusability [70–75]. The FESEM and TEM images of the DS-$Zn_{0.46}Cd_{0.54}S$ hollow nanospheres collected after nine cycles have been shown in Fig. S15, which also confirms that these DS-$Zn_{0.46}Cd_{0.54}S$ hollow nanospheres are kept with similar size and morphologies even under irradiation for 54 h, demonstrating the good chemical stability of the as-prepared sample. The photocatalytic quantum yield (QY) of DS-$Zn_{0.46}Cd_{0.54}S$ was further investigated under different monochromatic light irradiation wavelengths (Fig. 5d). There is an obvious reduction in the QY with the increase of irradiation wavelength, which is in great agreement with the UV–vis DRS of the as-obtained DS-$Zn_{0.46}Cd_{0.54}S$ hollow nanosphere photocatalysts. The nanostructure with a double-shell cloud provides more reaction sites for the reduction of water molecules, and it might serve as an efficient photon trapping agent for high light absorption, resulting in a greatly enhanced H_2 evolution rate [76]. Moreover, simulated calculations were also conducted to illustrate the enhanced ability of the absorption

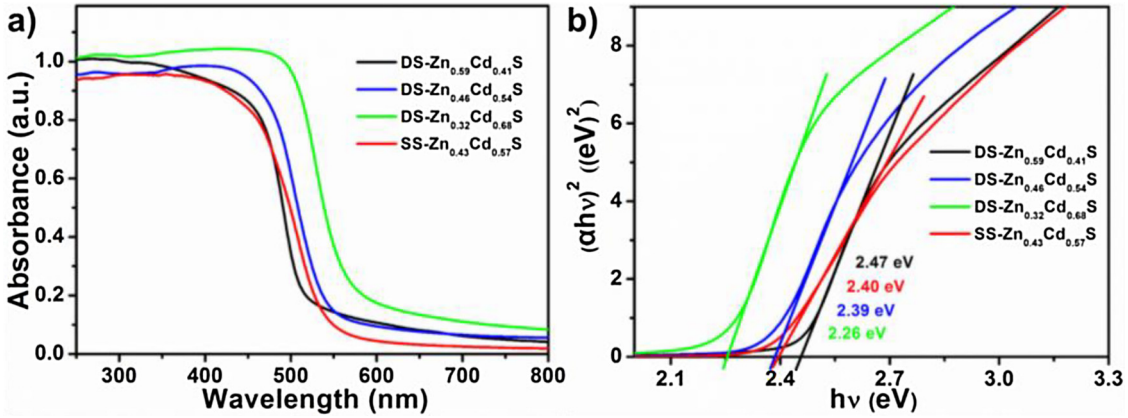

Fig. 4. (a) UV–vis diffuse reflectance spectra (DRS) of the as-obtained DS-$Zn_xCd_{1-x}S$ hollow nanospheres; (b) Kubelka-Munk plots showing the bandgap energy of the as-obtained $Zn_xCd_{1-x}S$ hollow nanospheres.

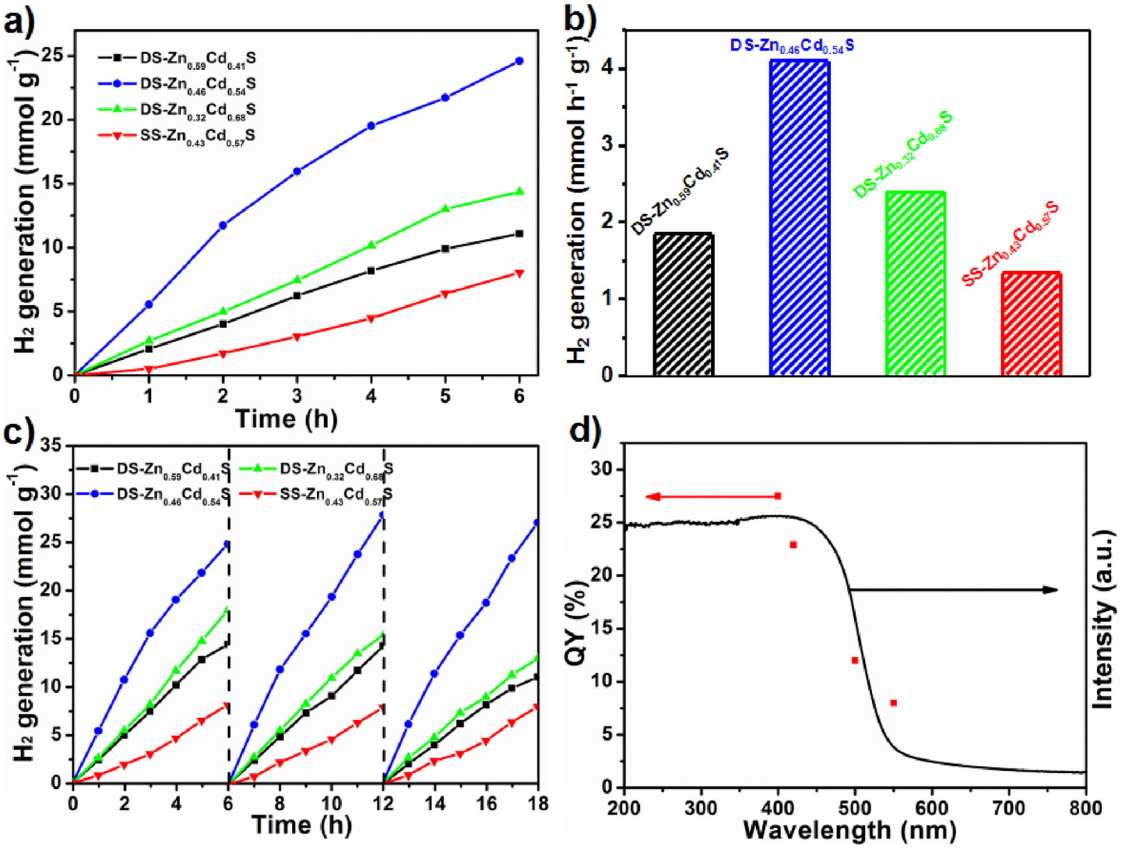

Fig. 5. (a, b) Time-dependent photocatalytic H_2 evolution and H_2 evolution rates from water over different samples. (c) Stability and reusability test under visible-light irradiation ($\lambda > 420$ nm) for 18 h, (d) QY along with the UV–vis absorption spectrum of DS-$Zn_{0.46}Cd_{0.54}S$.

and utilization of light in the presence of DS-$Zn_{0.46}Cd_{0.54}S$ hollow nanospheres [77]. As shown in Fig. S16, compared with the model of SS-$Zn_{0.43}Cd_{0.57}S$ hollow nanospheres, the transmittance rate of the model of DS-$Zn_{0.46}Cd_{0.54}S$ hollow nanospheres in the range of 370 nm–700 nm was obviously weakened while the reflectance and absorbance increased significantly. Meanwhile, the model of DS-$Zn_{0.46}Cd_{0.54}S$ hollow nanospheres has a resonance with double spherical shell, which led to a strong electric field local area and the strongest field was 493 V/m (Fig. S17b). In addition, the electric field of the model of SS-$Zn_{0.43}Cd_{0.57}S$ hollow without resonance was relatively weakened; resulting in the strongest field strength of the electric field was 260 V/m (Fig. S17a). On the basic of above analysis, the results of simulated calculations is consistent with the photocatalytic performance of $Zn_xCd_{1-x}S$ hollow nanospheres.

The photoluminescence (PL) spectrum is important to disclose the efficiency of photogenerated electron-hole pairs, carrier trapping, migration, transfer, separation and recombination, because PL emission mainly arises from the recombination of photoinduced electrons and holes for semiconductors [78]. Fig. 6a exhibited the PL emission spectra of $Zn_xCd_{1-x}S$ hollow nanospheres with the excitation wavelength of 360 nm. The peak intensity of DS-$Zn_xCd_{1-x}S$ hollow nanospheres is weaker than that of SS-$Zn_{0.43}Cd_{0.57}S$ hollow nanospheres owing to their thin shell with plentifully embedded mesopores that enhance the efficiency of charge transport across the surface, which suggests that the double-shell structure contributes to radiative recombination of photogenerated electron-hole pairs. Among all the samples, DS-$Zn_{0.46}Cd_{0.54}S$ hollow nanospheres display a drastically quenched PL peak that indicates the lowest photogenerated electron-hole recombination rate and thereby demonstrates the greatest photocatalytic hydrogen evolution activity.

Photoelectrochemical measurements are conducted to better understand and confirm the charge separation of these samples [79,80]. Fig. 6b Shows the transient and the periodic on/off photocurrent responses of the $Zn_xCd_{1-x}S$ hollow nanospheres photocatalyst loaded on fluorine doped tin oxide (FTO) electrodes measured under visible-light irradiation ($\lambda > 420$ nm). Apparently, for DS-$Zn_{0.46}Cd_{0.54}S$ hollow nanospheres sample, dramatically improvements of photocurrent density than other samples was observed, which can be attributed to both the efficient light utilization and the elevated separation efficiency of photogenerated electron-hole pairs [81,82]. It is noteworthy that attenuation trend of photocurrent value was consistent with the ability of hydrogen evolution. Furthermore, DS-$Zn_{0.46}Cd_{0.54}S$ hollow nanospheres remain a relative constant photocurrent value, which is consistent in the steady of photocatalytic performance.

Moreover, electrochemical impedance spectrum (EIS) were also used to evaluate the charge (photogenerated electrons and holes) transfer and recombination process for catalysts [83]. The EIS measurements (Fig. 6c, d) further demonstrate that the arc radius of DS-$Zn_{0.46}Cd_{0.54}S$ is smaller than those of DS-$Zn_{0.59}Cd_{0.41}S$, DS-$Zn_{0.32}Cd_{0.78}S$ and SS-$Zn_{0.43}Cd_{0.57}S$ photocatalysts under visible-light and dark, respectively. Thus, the as-obtained DS-$Zn_{0.46}Cd_{0.54}S$ double-shell hollow nanospheres possess more effective charge transfer and lower possibility of charge recombination,

Basing on the above characterization analysis and results, the possible underlying mechanism resulting in the high H_2 evolution rate is proposed in Scheme 2 for the DS- $Zn_xCd_{1-x}S$ photocatalyst with co-catalysts Pt under visible-light irradiation ($\lambda > 420$ nm). The double shell morphology displayed a higher total visible range absorption resulting from the multiple reflections and scattering of incident light in the double shell. Under visible light irradiation, these electrons in the VB of DS-$Zn_xCd_{1-x}S$ hollow nanospheres were excited to the CB while the photogenerated holes remained in the VB, producing electron-hole pairs [84]. The mesopores in the thin double shells effectively reduce the transfer distance between the interior and the surface of the

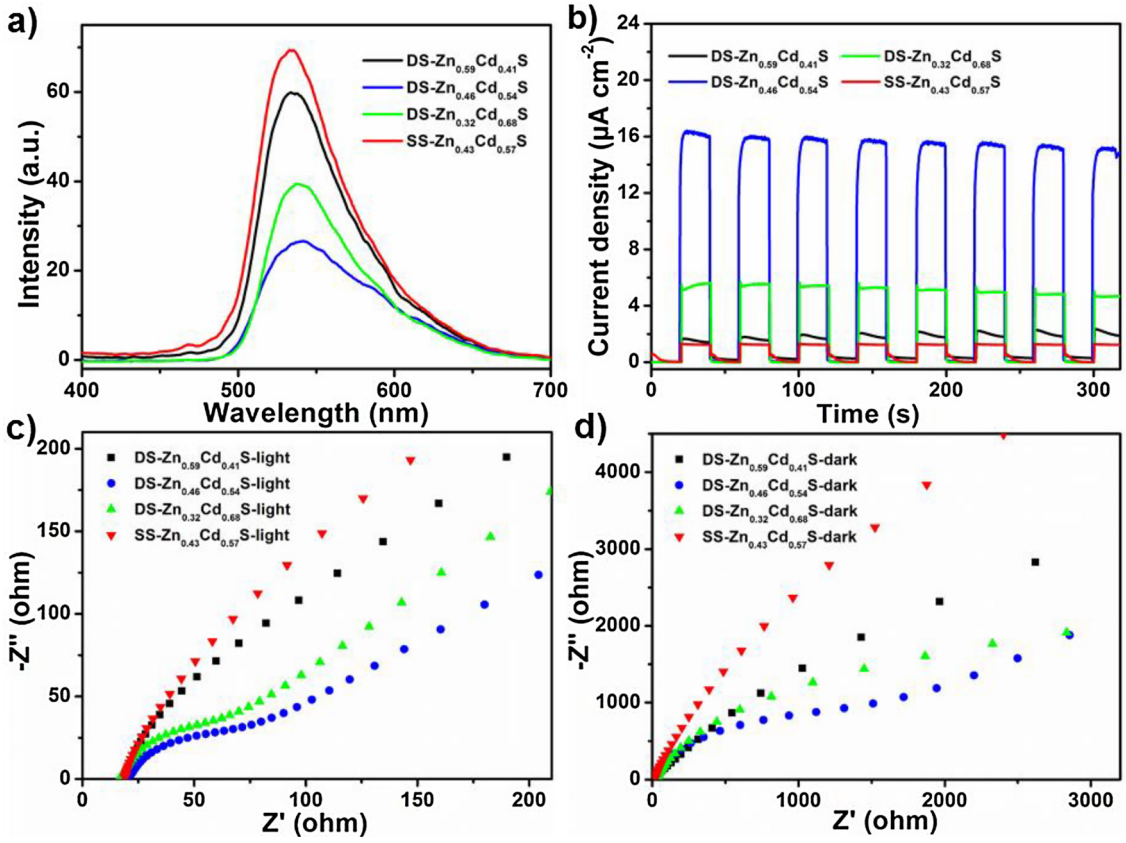

Fig. 6. (a) Photoluminescence spectra and (b) photocurrent responses of the as-obtained $Zn_xCd_{1-x}S$ hollow nanospheres; (c, d) EIS of the as-prepared products under visible-light illumination and in the dark, respectively.

catalyst, which drastically facilitates the charge separation efficiency. Meanwhile, the DS-prepared alloyed DS-$Zn_xCd_{1-x}S$ hollow nanospheres in this work possess a higher specific surface area that provides more reaction sites for the reduction of water molecules to generate H_2.

4. Conclusions

In conclusion, a sacrificial template strategy has been developed to fabricate alloyed $Zn_xCd_{1-x}S$ double-shell hollow nanospheres under hydrothermal condition using hierarchically porous ZnS nanospheres as hard templates. The formation mechanism and morphological evolution of the alloyed $Zn_xCd_{1-x}S$ double-shell hollow nanospheres have been studied carefully and can be attributed to the formation of alloyed hollow nanospheres via the solution-crystallization process of small nanoparticles of ZnS or $Zn_xCd_{1-x}S$. In addition, the chemical composition and void space for the double-shell hollow nanospheres can be modulated by controlling the concentration of $Cd(Ac)_2$. As expected, the as-prepared alloyed $Zn_xCd_{1-x}S$ double-shell hollow nanospheres exhibit excellent hydrogen production, and the H_2 evolution rate reaches as high as 4.11 mol h^{-1} g^{-1}. We believe the synthetic strategy that has been reported could be extended to construct other metal sulfide hollow nanostructures for various applications.

Acknowledgements

The authors would like toacknowledge funding from the National Natural Science Foundation of China (Grant 21471043, 21671173, 31501576). C. Zhang, H. Liu and W. Wang contributed equally to this

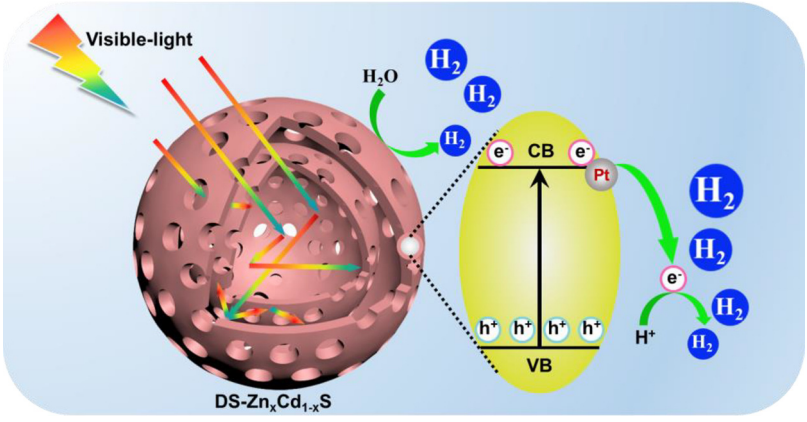

Scheme 2. Schematic description of photocatalytic H_2 production under irradiation of visible light.

work.

Appendix A. Supplementary data

Supplementary material related to this article can be found, in the online version, at doi:https://doi.org/10.1016/j.apcatb.2018.08.027.

References

[1] A.J. Brown, N.A. Brunelli, K. Eum, F. Rashidi, J. Johnson, W.J. Koros, C.W. Jones, S. Nair, Science 345 (2014) 72–75.
[2] J. Liu, G.Y. Jiang, Y. Liu, J.C. Di, Y.J. Wang, Z. Zhao, Q.Y. Sun, C.M. Xu, J.S. Gao, A.J. Duan, J. Liu, Y.C. Wei, Y. Zhao, L. Jiang, Sci. Rep. 4 (2014) 7276.
[3] G.L. Li, H. Mohwald, D.G. Shchukin, Chem. Soc. Rev. 42 (2013) 3628–3646.
[4] J. Qi, X.Y. Lai, J.Y. Wang, H.J. Tang, H. Ren, Y. Yang, Q. Jin, L.J. Zhang, R.B. Yu, G.H. Ma, Z.G. Su, H.J. Zhao, D. Wang, Chem. Soc. Rev. 44 (2015) 6749–6773.
[5] X.Y. Lai, J.E. Halpert, D. Wang, Energy Environ. Sci. 5 (2012) 5604–5618.
[6] Y. Li, J. Shi, Adv. Mater. 26 (2014) 3176–3205.
[7] J.B. Joo, M. Dahl, N. Li, F. Zaera, Y. Yin, Energy Environ. Sci. 6 (2013) 2082–2092.
[8] Y. Zhu, J. Shi, W. Shen, X. Dong, J. Feng, M. Ruan, Y. Li, Angew. Chem. Int. Ed. 117 (2005) 5213–5217.
[9] W.L. Chiang, C.J. Ke, Z.X. Liao, S.Y. Chen, F.R. Chen, C.Y. Tsai, Y. Xia, H.W. Sung, Small 8 (2012) 3584–3588.
[10] D. Yang, X. Kang, Y. Dai, Z. Hou, Z. Cheng, C. Li, J. Lin, Biomaterials 34 (2013) 1601–1612.
[11] R. Xing, A.A. Bhirde, S. Wang, X. Sun, G. Liu, Y. Hou, X. Chen, Nano Res. 6 (2013) 1–9.
[12] X.P. Fu, Q.K. Shen, D. Shi, K. Wu, Z. Jin, X. Wang, R. Si, Q.S. Song, C.J. Jia, C.H. Yan, Appl. Catal. B 211 (2017) 176–187.
[13] J. Qi, K. Zhao, G.D. Li, Y. Gao, H.J. Zhao, R.B. Yu, Z.Y. Tang, Nanoscale 6 (2014) 4072–4077.
[14] A.R. Jadhav, H.A. Bandal, H. Kim, Mater. Lett. 198 (2017) 50–53.
[15] F. Zhang, Y.Y. Wei, X.T. Wu, H.Y. Jiang, W. Wang, H.X. Li, J. Am. Chem. Soc. 136 (2014) 13963–13966.
[16] Y. Kuwahara, N. Furuichi, H. Seki, H. Yamashita, J. Mater. Chem. A Mater. Energy Sustain. 5 (2017) 18518–18526.
[17] S. Sadjadi, M. Malmir, M.M. Heravi, RSC Adv. 7 (2017) 36807–36818.
[18] H.T. Wang, W. Wang, Y.Y. Xu, S. Dong, J.W. Xiao, F. Wang, H.F. Liu, B.Y. Xia, ACS Appl. Mater. Interfaces 9 (2017) 10610–10617.
[19] C.L. Wang, L.S. Sun, F.F. Zhang, X.X. Wang, Q.J. Sun, Y. Cheng, L.M. Wang, Small 13 (2017) 1701246.
[20] D.P. Dubal, O. Ayyad, V. Ruiz, P. Gomez-Romero, Chem. Soc. Rev. 44 (2015) 1777–1790.
[21] Y. Jiao, Y. Zheng, M.T. Jaroniec, S.Z. Qiao, Chem. Soc. Rev. 44 (2015) 2060–2086.
[22] T.Y. Ma, S. Dai, S.Z. Qiao, Mater. Today 19 (2016) 265–273.
[23] A. Manthiram, Y.Z. Fu, S.H. Chung, C.X. Zu, Y.S. Su, Chem. Rev. 114 (2014) 11751–11787.
[24] M.V. Reddy, G.V.S. Rao, B.V.R. Chowdari, Chem. Rev. 113 (2013) 5364–5457.
[25] S.C. Kishore, S. Anandhakumar, M. Sasidharan, Appl. Surf. Sci. 400 (2017) 90–96.
[26] Z.N. Tetana, S.D. Mhlanga, N.J. Coville, Diamond Relat. Mater. 74 (2017) 70–80.
[27] Q. Chen, P.P. Yu, W.Q. Huang, S.C. Yu, M.H. Liu, C.J. Gao, J. Membr. Sci. 492 (2015) 312–321.
[28] P.K. Mishra, R. Wimmer, Ultrason. Sonochem. 35 (2017) 45–50.
[29] C. Liu, W.X. Fang, S.R. Chou, L. Shi, A.G. Fane, R. Wang, Desalination 308 (2013) 147–153.
[30] B. Mu, P. Liu, A.Q. Wang, Electrochim. Acta 88 (2013) 177–183.
[31] C. Yang, P. Liu, Ind. Eng. Chem. Res. 51 (2012) 13346–13353.
[32] W.B. Zhang, B. Mu, A.Q. Wang, J. Mater. Sci. 48 (2013) 7581–7586.
[33] Y.F. Zhang, C. Chen, J.G. Wang, L.N. Zhang, Carbohydr. Polym. 96 (2013) 528–535.
[34] S. Xiong, H.C. Zeng, Angew. Chem. Int. Ed. 51 (2012) 949–952.
[35] J. Pei, G. Chen, D.C. Jia, Y.G. Yu, J.X. Sun, Z.Z. Qiu, Y. Yu, RSC Adv. 4 (2014) 36257–36261.
[36] Y.J. Wang, L.P. Li, G.S. Li, RSC Adv. 2 (2012) 12999–13006.
[37] M. Sasidharan, K. Nakashima, Acc. Chem. Res. 47 (2014) 157–167.
[38] J. Jung-Konig, M. Sanhaji, R. Popescu, C. Seidl, E. Zittel, U. Schepers, D. Gerthsen, I. Hilger, C. Feldmann, Nanoscale 9 (2017) 8362–8372.
[39] N. Jatupaiboon, Y.F. Wang, H. Wu, X.J. Song, Y.Z. Song, J.B. Zhang, X.J. Ma, M.Q. Tan, J. Mater. Chem. B Mater. Biol. Med. 3 (2015) 3130–3133.
[40] C.H. Lin, J.H. Chang, Y.Q. Yeh, S.H. Wu, Y.H. Liu, C.Y. Mou, Nanoscale 7 (2015) 9614–9626.
[41] C. Mille, R.W. Corkery, J. Mater. Chem. A Mater. Energy Sustain. 1 (2013) 1849–1859.
[42] Y. Munaiah, B.G.S. Raj, T.P. Kumar, P. Ragupathy, J. Mater. Chem. A Mater. Energy Sustain. 1 (2013) 4300–4306.
[43] B.Y. Guan, L. Yu, X. Wang, S. Song, X.W. Lou, Adv. Mater. 29 (2017) 1605902.
[44] G. Zhang, X.W. Lou, Angew. Chem. Int. Ed. 126 (2014) 9187–9190.
[45] Z.M. Li, X.Y. Lai, H. Wang, D. Mao, C.J. Xing, D. Wang, J. Phys. Chem. C 113 (2009) 2792–2797.
[46] Z.H. Dong, X.Y. Lai, J.E. Halpert, N.L. Yang, L.X. Yi, J. Zhai, D. Wang, Z.Y. Tang, L. Jiang, Adv. Mater. 24 (2012) 1046–1049.
[47] H. Ren, R.B. Yu, J.Y. Wang, Q. Jin, M. Yang, D. Mao, D. Kisailus, H.J. Zhao, D. Wang, Nano Lett. 14 (2014) 6679–6684.
[48] J.Y. Wang, N.L. Yang, H.J. Tang, Z.H. Dong, Q. Jin, M. Yang, D. Kisailus, H.J. Zhao, Z.Y. Tang, D. Wang, Angew. Chem. Int. Ed. 52 (2013) 6417–6420.
[49] S.M. Xu, C.M. Hessel, H. Ren, R.B. Yu, Q. Jin, M. Yang, H.J. Zhao, D. Wang, Energy Environ. Sci. 7 (2014) 632–637.
[50] J.Y. Wang, H.J. Tang, H. Ren, R.B. Yu, J. Qi, D. Mao, H.J. Zhao, D. Wang, Adv. Sci. 1 (2014) 1400011.
[51] Z.H. Dong, H. Ren, C.M. Hessel, J.Y. Wang, R.B. Yu, Q. Jin, M. Yang, Z.D. Hu, Y.F. Chen, Z.Y. Tang, H.J. Zhao, D. Wang, Adv. Mater. 26 (2014) 905–909.
[52] J. Wang, H. Tang, L. Zhang, H. Ren, R. Yu, Q. Jin, J. Qi, D. Mao, M. Yang, Y. Wang, Nat. Energy 1 (2016) 16050.
[53] X. Zhao, R. Yu, H. Tang, D. Mao, J. Qi, B. Wang, Y. Zhang, H. Zhao, W. Hu, D. Wang, Adv. Mater. 29 (2017) 1700550.
[54] L. Yu, L. Zhang, H.B. Wu, X.W. Lou, Angew. Chem. Int. Ed. 126 (2014) 3785–3788.
[55] Y.M. Chen, Z. Li, X.W. Lou, Angew. Chem. Int. Ed. 127 (2015) 10667–10670.
[56] H. Hu, B.Y. Guan, X.W. Lou, Chem 1 (2016) 102–113.
[57] L. Shen, L. Yu, H.B. Wu, X.Y. Yu, X. Zhang, X.W. Lou, Nat. Commun. 6 (2015) 6694.
[58] G.R. Cai, H.L. Jiang, Angew. Chem. Int. Ed. 56 (2017) 563–567.
[59] Z. Chen, Y.T. Peng, F. Liu, Z.Y. Le, J. Zhu, G.R. Shen, D.Q. Zhang, M.C. Wen, S.N. Xiao, C.P. Liu, Y.F. Lu, H.X. Li, Nano Lett. 15 (2015) 6802–6808.
[60] X.F. Wang, Y.H. Tang, P.H. Shi, J.C. Fan, Q.J. Xu, Y.L. Min, Chem. Eng. J. 334 (2018) 1642–1649.
[61] H.H. Wei, Q. Zhang, Y. Wang, Y.J. Li, J.C. Fan, Q.J. Xu, Y.L. Min, Adv. Funct. Mater. 28 (2018) 1704440.
[62] R.W. Liang, F.F. Jing, G.Y. Yan, L. Wu, Appl. Catal. B 218 (2017) 452–459.
[63] W.N. Wang, C.X. Huang, C.Y. Zhang, M.L. Zhao, J. Zhang, H.J. Chen, Z.B. Zha, T.T. Zhao, H.S. Qian, Appl. Catal. B 224 (2018) 854–862.
[64] M.L. Zhao, W.N. Wang, C.X. Huang, W. Dong, Y. Wang, S. Cheng, H.Q. Wang, H.S. Qian, Chin. J. Catal. 39 (2018) 1240–1248.
[65] J.F. Qian, P. Liu, Y. Xiao, Y. Jiang, Y.L. Cao, X.P. Ai, H.X. Yang, Adv. Mater. 21 (2009) 3663–3667.
[66] Z.P. Tian, H.M. Tian, X.Y. Wang, S.K. Yuan, J.Y. Zhang, X.B. Zhang, T. Yu, Z.G. Zou, Appl. Phys. Lett. 94 (2009) 031905.
[67] J. Chen, B.B. Ding, T.Y. Wang, F. Li, Y. Zhang, Y.L. Zhao, H.S. Qian, J. Mater. Sci. - Mater. Electron. 25 (2014) 4103–4109.
[68] J. Boltersdorf, I. Sullivan, T.L. Shelton, Z.K. Wu, M. Gray, B. Zoellner, F.E. Osterloh, P.A. Maggard, Chem. Mater. 28 (2016) 8876–8889.
[69] A. Etogo, R. Liu, J.B. Ren, L.W. Qi, C.C. Zheng, J.Q. Ning, Y.J. Zhong, Y. Hu, J. Mater. Chem. A Mater. Energy Sustain. 4 (2016) 13242–13250.
[70] I. Lee, J.B. Joo, Y.D. Yin, F. Zaera, Angew. Chem. Int. Ed. 50 (2011) 10208–10211.
[71] Q.J. Xiang, J.G. Yu, M. Jaroniec, J. Am. Chem. Soc. 134 (2012) 6575–6578.
[72] F.K. Meng, J.T. Li, S.K. Cushing, M.J. Zhi, N.Q. Wu, J. Am. Chem. Soc. 135 (2013) 10286–10289.
[73] L. Yang, D. Zhong, J.Y. Zhang, Z.P. Yan, S.F. Ge, P.W. Du, J. Jiang, D. Sun, X.J. Wu, Z.Y. Fan, S.A. Dayeh, B. Xiang, ACS Nano 8 (2014) 6979–6985.
[74] D.Q. Zhang, P.J. Liu, S.N. Xiao, X.F. Qian, H. Zhang, M.C. Wen, Y. Kuwahara, K. Mori, H.X. Li, H. Yamashita, Nanoscale 8 (2016) 7749–7754.
[75] X.R. Cao, G.H. Tian, Y.J. Chen, J. Zhou, W. Zhou, C.G. Tian, H.G. Fu, J. Mater. Chem. A Mater. Energy Sustain. 2 (2014) 4366–4374.
[76] Z.W. Tong, D. Yang, Z. Li, Y.H. Nan, F. Ding, Y.C. Shen, Z.Y. Jiang, ACS Nano 11 (2017) 1103–1112.
[77] W.B. Sun, Q. Fu, Z.Z. Chen, Appl. Opt. 38 (1999) 3141–3151.
[78] J.R. Ran, T.Y. Ma, G.P. Gao, X.W. Du, S.Z. Qiao, Energy Environ. Sci. 8 (2015) 3708–3717.
[79] H.L. Tan, A. Suyanto, A.T. De Denko, W.H. Saputera, R. Amal, F.E. Osterloh, Y.H. Ng, Part. Part. Syst. Charact. 34 (2017) 1600290.
[80] R. Liu, J.B. Ren, D. Zhao, J.Q. Ning, Z.Y. Zhang, Y.J. Wang, Y.J. Zhong, C.C. Zheng, Y. Hu, Inorg. Chem. Front. 4 (2017) 2045–2054.
[81] B. He, R. Liu, J.B. Ren, C.J. Tang, Y.J. Zhong, Y. Hu, Langmuir 33 (2017) 6719–6726.
[82] H.W. Huang, S.C. Tu, C. Zeng, T.R. Zhang, A.H. Reshak, Y.H. Zhang, Angew. Chem. Int. Ed. 56 (2017) 11860–11864.
[83] X.L. Yu, R.F. Du, B.Y. Li, Y.H. Zhang, H.J. Liu, J.H. Qu, X.Q. An, Appl. Catal. B 182 (2016) 504–512.
[84] S.N. Xiao, P.J. Liu, W. Zhu, G.S. Li, D.Q. Zhang, H.X. Li, Nano Lett. 15 (2015) 4853–4858.